Biophysical Chemistry xxx (xxxx) 107292

Contents lists available at ScienceDirect

Biophysical Chemistry

journal homepage: www.elsevier.com/locate/biophyschem

Calcium ions do not influence the Aβ (25–35) triggered morphological changes of lipid membranes

Sergei Kurakin [a, b, *], Oleksandr Ivankov [a], Ermuhammad Dushanov [c, d], Tatiana Murugova [a], Elena Ermakova [a], Sergey Efimov [b], Timur Mukhametzyanov [e], Svetlana Smerdova [f], Vladimir Klochkov [b], Alexander Kuklin [a, g], Norbert Kučerka [a, h, *]

[a] Frank Laboratory of Neutron Physics, Joint Institute for Nuclear Research, Joliot-Curie 6, Dubna, Moscow Region 141980, Russia
[b] Institute of Physics, Kazan Federal University, Kremlevskaya 18, Kazan 420008, Russia
[c] Laboratory of Radiation Biology, Joint Institute for Nuclear Research, Joliot-Curie 6, Dubna, Moscow Region 141980, Russia
[d] Department of Biophysics, Dubna State University, Universitetskaya 19, Dubna, Moscow Region 141982, Russia
[e] Butlerov Chemistry Institute, Kazan Federal University, Kremlevskaya 18, Kazan 420008, Russia
[f] Kazan National Research Technological University, Karl Marx 68, Kazan 420015, Russia
[g] Moscow Institute of Physics and Technology, Instytutskiy Pereulok 9, Dolgoprudny, Moscow Region 141701, Russia
[h] Department of Physical Chemistry of Drugs, Faculty of Pharmacy, Comenius University Bratislava, Odbojárov 10, Bratislava 832 32, Slovakia

ARTICLE INFO

Keywords:
Amyloid-beta peptide
Unilamellar vesicles
Bicelle-like structures
Small-angle X-ray scattering
Small-angle neutron scattering
Nuclear magnetic resonance

ABSTRACT

We have studied the effect of calcium ions (Ca^{2+}) at various concentrations on the structure of lipid vesicles in the presence of amyloid-beta peptide Aβ (25–35). In particular, we have investigated the influence of calcium ions on the formation of recently documented bicelle-like structures (BLSs) emerged as a result of Aβ (25–35) triggered membrane disintegration. First, we have shown by using small-angle X-ray and neutron scattering that peptide molecules rigidify the lipid bilayer of gel phase DPPC unilamellar vesicles (ULVs), while addition of the calcium ions to the system hinders this effect of Aβ (25–35). Secondly, the Aβ (25–35) demonstrates a critical peptide concentration at which the BLSs reorganize from ULVs due to heating and cooling the samples through the lipid main phase transition temperature (T_m). However, addition of calcium ions does not affect noticeably the Aβ-induced formation of BLSs and their structural parameters, though the changes in peptide's secondary structure, e.g. the increased α-helix fraction, has been registered by circular dichroism spectroscopy. Finally, according to ^{31}P nuclear magnetic resonance (NMR) measurements, calcium ions do not affect the lipid-peptide arrangement in BLSs and their ability to align in the magnetic field of NMR spectrometer. The influences of various concentrations of calcium ions on the lipid-peptide interactions may prove biologically important because their local concentrations vary widely in in-vivo conditions. In the present work, calcium ions were investigated as a possible tool aimed at regulating the lipid-peptide interactions that demonstrated the disruptive effect of Aβ (25–35) on lipid membranes.

1. Introduction

A full-length amyloid-beta peptide (Aβ) is known to be cleaved enzymatically from a transmembrane amyloid precursor protein (APP) in 1–40 and 1–42 isoforms (Aβ (1–40) and Aβ (1–42) correspondingly), which are supposed to be the prime cause of the onset of Alzheimer's disease (AD) [1]. A short amyloid-beta peptide Aβ (25–35) consisting of 11 amino acids is reported to be one of the most toxic fragments of full-length amyloid-beta peptide [2]. Aβ (25–35) molecules, also found in brains of AD patients [3], reproduce its main toxic properties, such as tendency to the fast aggregation in different environment accompanied with the fibril or oligomer formation [4–6], damage of DNA molecules [7], and neuronal apoptosis [8–10].

Calcium ions may play an important role in the progression of AD and in emerging of the Aβ-peptide pathological properties. Several studies have shown that calcium ions accelerate the aggregation of Aβ-peptides in solution. For example, physiologically relevant concentrations of calcium ions (2 mM) induce the aggregation of Aβ-peptides, which tend to form β-sheets with the subsequent growth of oligomers and fibrils [11,12]. Elevated calcium ion concentrations around the Aβ

* Corresponding authors at: Frank Laboratory of Neutron Physics, Joint Institute for Nuclear Research, Joliot-Curie 6, Dubna, Moscow Region 141980, Russia.
E-mail addresses: Sergej.Kurakin@nf.jinr.ru (S. Kurakin), kucerka@nf.jinr.ru (N. Kučerka).

https://doi.org/10.1016/j.bpc.2024.107292
Received 6 March 2024; Received in revised form 4 July 2024; Accepted 9 July 2024
0301-4622/

aggregates have been detected in brains of AD patients, suggesting possibly a significant role in AD development [13,14]. Regarding the interactions of Aβ-peptides with cells in the presence of calcium ions, it is known that the peptides can lead to dysregulations of intracellular concentrations of calcium ions. This happens not only due to the activation of calcium channels [15] by specific interactions between peptide molecules and neuronal receptors on the membrane [16], but also due to formation of ion channels inside the cell membranes by peptides themselves. It leads to the uncontrolled influx of calcium ions from the extracellular environment into the cell [17,18]. On the other hand, increase of the calcium concentration was able to block the formation of amyloid channels in lipid membranes and subsequent membrane damage [19]. Finally, the presence of calcium ions has also been reported to stimulate the growth of amyloid fibers on the lipid membrane surface [19,20]. Importantly, formation of ion channels in membranes was also proposed in the case of Aβ (25–35) peptides [21,22]. The structure of such Aβ (25–35) channels in lipid membranes was found to be represented mostly by several amyloid molecules in an oligomeric state [23].

More recently, the investigations of amyloid toxicity have refocused their attention from large extracellular fibrils to the membrane-modulated actions of peptides embedded therein. Dysregulations of many cellular processes are known to be affected by the membrane composition, molecular surroundings, and protein concentration. Meanwhile, thermodynamic phase of a lipid membrane is also among the important factors, as it is supposed to affect fluidity and structure of lipid membranes [24,25]. Recently, we have observed the ability of Aβ (25–35) monomers incorporated into the lipid bilayer to trigger morphological reorganization of lipid membranes during the changes in the thermodynamic state of the membrane from the lipid gel phase to its fluid phase [26–29]. Namely, the reorganization between planar bicelle-like structures (BLSs) and spherical unilamellar vesicles (ULVs) has been reported when crossing the main phase transition temperature (T_m) of lipids (see Supplementary material, Fig. S1). This effect of the Aβ (25–35) driven membrane reorganization has been described for fully saturated zwitterionic dipalmitoylphosphatidylcholine (DPPC) or dimyristoylphosphatidylcholine (DMPC) lipids [26,29], as well as those with the addition of negatively charged lipid head groups [27], cholesterol, and melatonin molecules [28]. This reorganization was concluded to be a result of a temporal disintegration of the lipid membrane by monomeric Aβ (25–35) molecules, demonstrating thus their disruptive properties during the lipid main phase transition. Changes to the membrane fluidity were suggested to be the main factor promoting Aβ (25–35) molecules to reorganize the lipids in these systems. Though the saturated lipids, DPPC in particular, are the most relevant components of lung surfactant [30], they are widespread also in the brain tissues [31]. Their abundance there reaches up to 30–50% of all phosphatidylcholines (PC), with the second most abundant lipid being mixed-chain POPC (C16:0,18:1PC) at the comparable amounts [32,33]. Brain lipids are relatively highly enriched also in polyunsaturated fatty acids, mostly in the case of phosphatidylethanolamine lipids while $<5\%$ in the case of PCs [32].

The niche of our studies is investigating the pre-clinical stages of AD by modeling the system with Aβ (25–35) peptides incorporated in the membrane. We choose the 25–35 fragment because it is an APP transmembrane segment [34,35] allowing to study the lipid-peptide interactions and its location in the membrane, while it exhibits cytotoxic properties similar to the full-length peptide [36]. In the current work, Aβ (25–35) molecules are incorporated in the membrane during the sample preparation and according to our results they most likely do not escape the membrane during the entire course of our measurements. This is supported by absence of peptide aggregates outside the membranes and presence of reversible morphological changes. Also, the recently revealed arrangement of BLS supports the idea of non-aggregated peptides incorporated in the membrane while mixed with lipids at the rim of BLSs [29].

In the present study, we focus on the role of calcium ions via their addition to the solvent. We investigate the effect of calcium ions on the lipid membrane morphological reorganizations occurring at the verge of the lipid gel phase (BLS and ULV morphologies in particular) - the morphological changes caused by Aβ (25–35). Demonstrating no specific binding to the Aβ-monomers [37], calcium ions are among the effective biological modulators of lipid membrane structure [38–41]. They strongly bind to lipids altering their conformations, dynamics, and structural ordering [42–47]. A millimolar range of calcium ion concentrations was found to alter the structural parameters of lipid membranes demonstrating several peculiarities in the bilayer thickness and vesicle size [38–40,48–50]. Thus, we accentuate our attention on the emergence of BLSs in the lipid gel phase as a result of Aβ(25–35)-induced membrane disintegration and correlate it with the effect of calcium ions on the lipid bilayer structure. As peptide-induced changes of the structure of lipid membranes and their disintegration are relevant for understanding the origins of AD development, we use the small angle X-ray scattering (SAXS), small angle neutron scattering (SANS), molecular dynamics (MD) simulations, and ^{31}P nuclear magnetic resonance (NMR) spectroscopy to evaluate the structural parameters of lipid membranes upon increasing concentration of calcium ions and to unravel general shape and lipid-peptide arrangement in emerged lipid objects (BLSs and ULVs). At the same time, the circular dichroism (CD) spectroscopy is used to study the peptide secondary structure in BLSs when adding calcium ions.

2. Materials and methods

2.1. Sample preparation

1,2-Dipalmitoyl-*sn*-glycero-3-phosphocholine (DPPC), 1,2-dimyristoyl-*sn*-glycero-3-phosphocholine (DMPC) from Avanti Polar Lipids (Alabaster, AL), and amyloid-beta peptide fragment 25–35, Aβ (25–35) (purity $>95\%$ by HPLC), from Abbiotec (Escondido, CA) were purchased in powder form and used without further purification. Organic solvents of 2,2,2-trifluoroethanol (TFE) and chloroform, as well as 2,2,2-trifluoroacetic acid (TFA) and salt of $CaCl_2{\cdot}2H_2O$ were purchased from Sigma Aldrich (Russia). Ultrapure H_2O (18.2 MΩcm at 25 °C) was obtained from the MilliQ purification system.

Lyophilized Aβ (25–35) peptide was dissolved in TFA and treated in the ultrasonic bath for 5 min in order to avoid the peptide aggregation [51]. Aliquots of acid were distributed into vials to reach the desired peptide concentration for final samples. Acid was then evaporated from each vial under a stream of nitrogen and dried under vacuum for ~15 h. The efficiency of procedure for preparing non-aggregated Aβ (25–35) peptide samples was confirmed by examining the selected samples dispersed without lipid environment in water solution with or without calcium ions using the CD spectroscopy (see Supplementary material, Fig. S2).

Lipid powders were dissolved in the organic solvent mixture of chloroform:TFE taken in ratio of 1:1 (vol/vol) at the total lipid concentration of 90 mg/ml for DPPC and 20 mg/ml for DMPC. The mixture of lipids and organic solvents was added to the vials with peptide for obtaining lipid-peptide samples. The lipid and lipid-peptide mixtures in organic solvents were then evaporated in the CentriVap® Centrifugal Concentrator equipped with a Cold Trap (Labconco, USA) and exposed to vacuum overnight for removing traces of the remaining solvent.

The lipid and lipid-peptide films were hydrated with H_2O (for SAXS and CD measurements), D_2O (for SANS measurements), or with the mixture of H_2O and D_2O (for NMR measurements) at the desired concentrations of calcium ions in the range of 0–50 mM prepared as stock solutions. Total lipid concentrations were equal to 0.5 wt% (7.4 mM DMPC for CD measurements), 1 wt% (13.6 mM DPPC for SAXS and SANS), 5 wt% (68.1 mM DPPC for NMR experiments). The peptide/lipid fraction was equal to the range of 0.01–5 mol% (SAXS and SANS

experiments), 1 mol% (for NMR experiments) and 3 mol% (for CD experiments). The hydrated samples were subjected to 7–8 freeze-thaw cycles accompanied with a thorough vortexing and shaking. This process is supposed to create a sample consisting of regularly hydrated multilamellar vesicles (MLVs). The peptide/lipid fraction was selected relatively low (≤ 5 mol%) to avoid a spontaneous aggregation of Aβ (25–35) peptide in lipid bilayers [26,35].

Samples needed for SAXS and SANS experiments were further subjected to the following procedure. The resulting solution of dispersed MLVs was extruded. The extrusion was performed by using the Avanti Mini Extruder® (Avanti Polar Lipids, AL) fitted with polycarbonate membranes of pore size 500 Å (for SAXS experiments) leading to formation of the unilamellar vesicles. The samples were subjected to 31 passes through the filter. Further, the samples were measured by means of SAXS and SANS. After the measurements, the samples were subjected to 3 heating-cooling cycles between 10 and 60 °C (below and above T_m of lipids) being exposed to the limit temperatures for 8–10 h. This manipulation ensures the stability of the samples, as well as formation of small ULVs above T_m and BLSs below T_m by peptide-induced breakage of lipid bilayers at suitable Aβ (25–35) concentrations [26].

The separate samples for NMR and CD experiments were subjected to the same heating-cooling cycles right after hydration by buffer (without extrusion). This manipulation is alternative to the extrusion as it promotes the MLV disintegration by peptide-induced breakage of lipid bilayers [29].

2.2. SAXS measurements

SAXS measurements were performed on the Xenocs Xeuss 3.0 SAXS/WAXS instrument (FLNP JINR, Dubna, Russia). The spectrometer has a GeniX 3D microfocus X-ray generator with a copper anode, at a voltage of 50 kV and a current of 0.6 mA with a power of 30 W. The SAXS instrument also has a vacuum tube equipped with the moving detector Eiger2 R1 M with a sensitive area of 77.1 × 79.7 mm^2, where the pixel linear size is equal to 75 μm. All sample measurements were carried out at two detector positions – at the sample-detector distances of 350 mm and 1800 mm to cover the q range of 0.005 $Å^{-1}$–0.75 $Å^{-1}$. The samples were placed in the 2-mm-thick round glass capillaries (Hilgenberg GmbH, Germany) and measured at T = 20 °C, while data accumulation at each detector position was 1 h. Intensity calibration was performed using the calibration samples of silver behenate and amorphous carbon.

After measurements, the 2D scattering patterns obtained from the detector were processed by the XSACT 2.4 program to obtain one-dimensional scattering curves. The collected curves were also corrected for background scattering from the buffer solution. The final SAXS curves were fitted using the SASfit 0.94.11 software package [52]. We have used a fitting model containing form-factor of a thin sphere (or a thin disk) describing a unilamellar vesicle (or a bicelle-like structure) combined with form-factor of a lipid bilayer represented by 3 G functions. From the fitting, we were able to obtain the radii of vesicles described by the thin sphere (R_{ULV}) and radii of BLSs described by the thin disk (R_{BLS}). The fitting expressions for SAXS curves are presented in Supplementary Material.

2.3. SANS measurements

SANS experiments were performed on the time-of-flight small-angle neutron scattering spectrometer YuMO, located at the IBR-2 pulsed nuclear reactor (FLNP JINR, Dubna, Russia) serving as the source of neutrons [53]. A beam of cold neutrons with a cold-moderator setup [54] or a beam of thermal neutrons was adjusted by a set of two pinhole collimators with diameters of 40 and 14 mm and directed onto the samples. The neutrons scattered from the samples were recorded by two gas-filled ring detectors located at distances of 4.5 m and 13 m from the sample position. Such geometry made it possible to cover the range of the scattering vector q from 0.007 $Å^{-1}$ to 0.5 $Å^{-1}$, where $q = (4\pi/\lambda)\sin(\theta/2)$, λ is the wavelength and θ is the scattering angle. The lower limit of q-range was extended to 0.005 $Å^{-1}$ in the case of cold neutrons.

The samples were placed in the 1-mm-thick flat quartz cuvettes from Hellma (Germany) and held in the multipositional sample holder connected to the Lauda liquid thermostat. The device has a temperature controller Pt-100 that allows for a temperature accuracy of ±0.03 °C. The vanadium standard was used to calibrate the absolute scattering intensity, while the blank buffer solution was used to calibrate the background intensity. The accumulation of SANS data took 15–20 min.

The treatment of raw data from detectors was performed in the SAS program [55]. The resulting neutron scattering curves were analyzed by OriginPro 2018 software utilizing the models described in the Supplementary Material. The Kratky-Porod model described by a single parameter of Gibbs-Luzatti bilayer thickness (d_L) was used [56,57]. The uncertainties of fitted parameters were calculated from the covariance matrix multiplied by the square-root of normalized chi-square.

2.4. Molecular dynamics simulations

Molecular dynamics (MD) simulations on the lipid membrane systems were performed using the Gromacs package [58]. Our base membrane system consisted of 242 DPPC molecules solvated with 12,100 TIP3 water molecules. The original topology was taken from CHARMM-GUI_v1.9, while MD modeling was carried out in three stages: the energy minimization, NVT and NPT relaxation procedures. All the MD calculations were carried out with a CHARMM36m force field with the full atomic interaction approach [59].

The systems containing lipid, Aβ (25–35) molecules, and ions were formed using CHARMM-GUI and additional simulation packages, such as VMD, Chimera, and Pymol [60,61]. The systems were constructed with the lipid:Aβ ratio of 242:7 (3 mol% Aβ) and lipid:Ca^{2+} ratio of 242:24 to enforce a close correlation with experimental conditions.

All covalent bonds in our simulated systems were limited by the LINCS algorithm. The Lennard-Jones interaction calculations were processed using a force-based switching algorithm started at 10 Å using cutoff at 12 Å. The electrostatics calculations were performed by Ewald method with a cut-off radius of 12 Å. The periodic boundary conditions were used in all three dimensions. The integration of the equations of motion was done using a modified Verlet algorithm with a time step of 1 fs under a radius of 12 Å. The preparation stage (energy minimization, NVT and NPT equilibration) were carried out for 10 ns. In the system balancing, we have used a Berendsen thermostat at the temperature of 293.15 K for the NVT and NPT ensembles, as well as a semi-isotropic Berendsen barostat for a pressure balancing at 1 bar for the NPT ensemble. The production simulations were carried out in the NPT ensemble with a Nose-Hoover thermostat at 293.15 K and a Parrinello-Rahman barostat at 1 bar for 100 ns, while assessing their equilibration via surveying the area per lipid. The temperature and pressure of the entire system (membrane and water solvent) were connected independently to each other. All simulations were carried out under the full hydration mode (i.e., >30 water molecules per lipid).

The analysis of simulation results was focused on obtaining the averaged distributions of various components. We employed the inhouse software SIMtoEXP [62] for reconstructing the electron density profiles (EDP) of the DPPC lipid bilayer and Aβ (25–35) molecules from the simulated results. Namely, the simulation results are first averaged laterally by binning the z location of various atoms. The bin size was about 0.2 Å and the atoms were grouped into functional groups defined according to the SDP model [63] (PCN – phosphate and CH_2CH_2N, $CholCH_3$ – three choline CH_3 groups, CG – carbonyl and glycerol, CH_2 – lipid chains methylene groups, CH_3 – terminal methyls, water, Aβ (25–35), and calcium and chlorine ions). The electron density of each group was normalized by the number of electrons occurring in the

given group. The results are then obtained in the form of 1D electron density distributions.

2.5. ^{31}P NMR spectroscopy

^{31}P NMR experiments were performed on the Bruker AVANCE II NMR spectrometer with a working proton frequency of 500 MHz. The spectra were collected at the 202.46 MHz frequency for ^{31}P using the zgpg30 pulse sequence with proton decoupling. The duration of pulses was 15 μs with 6-s recycle delay. The spectral width was set to 24.3 kHz, while exponential multiplication with the line broadening parameter of 100 Hz was applied prior to Fourier transformation. Acquisition time was 1.35 s. A total of 2000 signal transients were collected. Chemical shift was referenced to 0 ppm using 85% H_3PO_4. Samples were measured in the temperature range of 30–45 °C.

2.6. Circular dichroism spectroscopy

Circular dichroism (CD) spectra were collected with J-1500 CD spectrometer (JASCO International Co. Ltd., Tokyo, Japan). All measurements were performed with lipid-peptide systems enriched by calcium ions at various concentrations. The samples were loaded to the Hellma quartz cells with an optical pathlength of 1 mm. CD spectra were accumulated with 3 scans. We used wavelength range from 190 to 250 nm with a 0.5 nm step. Scanning speed was set to 20 nm/min, time per point 3.0 s, and bandwidth equal to 5 nm. The spectrum of the samples without added Aβ (25–35) peptide was used as a reference sample and its CD signal was subtracted from the spectra of studied samples. All CD spectra were normalized to the mean residue molar ellipticity [θ]. We have used the DichroWeb website [64] in order to calculate fraction of different peptide secondary structures from obtained CD spectra via CONTIN [65] deconvolution program while applying SMP180 set [66] of referential protein secondary structures.

3. Results and discussion

3.1. Effect of Aβ (25–35) peptides and calcium ions on the structure of lipid membranes in extruded unilamellar vesicles

SANS and SAXS techniques were used to determine the effect of calcium ions on the structural parameters of the DPPC membranes with amyloid-beta peptide incorporated. The membranes were prepared in the form of ULVs via extrusion procedure and examined first without further (thermal) manipulation for establishing their initial characteristics. We have focused particularly on the bilayer thicknesses (d_L) and vesicle radii (R_{ULV}) as main structural parameters of ULV systems. The samples were studied in a wide range of low peptide concentrations (0.01–5 mol% of peptide-in-lipid fractions) and concentrations of calcium ions (0–10 mM calcium ions in solutions) in the gel phase of DPPC at the temperature of 20 °C. Determination of the parameters was implemented by a model-based fitting of experimental small-angle scattering curves that is described in the Supplementary Material and Materials and Methods section. Briefly, the fitting model containing a form-factor of thin sphere describing the ULV was used in the case of SAXS, while SANS data were fitted by Kratky-Porod approximation related to the bilayer properties.

Fig. 1 shows the SAXS and SANS curves and their best-fit results of extruded DPPC(1 wt%) + Aβ (25–35) samples containing various concentrations of Aβ (25–35) molecules (Fig. 1a and b) and DPPC (1 wt%) + Aβ (25–35) + Ca^{2+} samples with different concentrations of calcium ions at constant Aβ (25–35)(1 mol%) content (Fig. 1c and d). This peptide concentration was chosen based on our previous observations of detectable impact of Aβ (25–35) on the morphological changes of membranes, yet avoiding the regime of peptide aggregation [26–29]. The model used in SAXS data analysis fits well to the curves over an entire q-range measured (Fig. 1a and c). These curves are characteristic by a pit at low q values (shown by black arrow at $q \approx 0.01$ Å^{-1}) that corresponds to the relatively large sizes in real space ($2\pi/q \approx 600$ Å) and provide thus best information about the ULV radii (R_{ULV}). The high q-range data ($q > 0.1$ Å^{-1}) may be used for describing the inner membrane structure when detailed models are employed, though this typically requires high-quality data up to $q \approx 0.5$ Å^{-1} and more [67,68]. We therefore focus on obtaining the former information that is contained in the low q-range (namely, R_{ULV}). We receive the information about the bilayer structure (its thickness d_L) from our SANS data analysis. The data and their best-fit results (Fig. 1b and d) display characteristically smooth curves, typical for samples with high polydispersity, that provide best the bilayer thickness parameter when Kratky-Porod approximation is employed [26].

For all the peptide and calcium ion concentrations studied, the SAXS and SANS curves have typical patterns of scattering on ULVs [50], and reveal the absence of Bragg peaks that would result from multilamellar vesicles (MLVs) even when comprising two lamellae only or in the case of MLV contamination as low as 5% [69–71]. Examining the effect of increasing peptide concentration first, we note a systematic shift of the pit described above (Fig. 1a marked by arrows) to the even smaller values of q. This indicates an increase in the R_{ULV} values with increasing peptide concentration in the samples without ions added. The quantitative results of scattering data analysis presented in Fig. 2 confirm the estimated trend of changes in R_{ULV} and complement it by the results of changes in d_L as a function of Aβ (25–35) concentration. Within the studied concentration interval, one can observe a systematic increase in the R_{ULV} by almost 100 Å (from 289 Å to 383 Å; Fig. 2a) and increase in the d_L by >4 Å (from 50.0 Å to 54.8 Å; Fig. 2b). The gradual increase in the structural parameters confirm incorporation of the Aβ (25–35) molecules into the lipid bilayer.

The increase in the size of ULVs can be explained by the fact that the Aβ (25–35) peptide molecules being embedded in the lipid bilayer regulate its elasto-mechanical properties by rigidifying the membrane. A rigid lipid membrane is characterized by higher bending modulus leading to the decreased bending ability of a membrane that defines its curvature in vesicles and therefore the vesicle size when extruding the samples. The direct correlation between the lipid bilayer rigidity and vesicle size was for example reported during vesiculation processes when adding cholesterol [28,72]. Elevated membrane rigidification upon peptide addition in our case is supported also by the increase in the lipid bilayer thickness, which is known to be an indicator of the impaired dynamics of hydrocarbon chains promoting their ordering [73]. Thus, the increase in the concentration of the Aβ (25–35) peptide in our case leads to the increase in rigidity of the lipid bilayer.

Intriguingly, the presence of calcium ions (2 mM) in the samples of similar content as above affects the influence of Aβ (25–35) on the R_{ULV} values. This can be recognized from the pattern of SAXS curves in Fig. S5, as well as from the qualitative results shown in Fig. 2a (red points). Under these circumstances, the ULV radius as a function of Aβ (25–35) concentration increases only slightly (≈ 30 Å) over the entire peptide concentration interval investigated. This observation of the obstructing effect of calcium ions on the effect of Aβ (25–35) on the membrane structural parameters prompted us to investigate such systems in the presence of calcium ions more closely.

We have scrutinized the series of samples based on the ULVs prepared of DPPC(1 wt%) + Aβ (25–35) at various concentrations of calcium ions, where Aβ (25–35) concentration was fixed to 1 mol%. The SAXS pattern (Figure 1c) reveals a shift of the low-q values pit towards the higher q-values while increasing concentration of calcium ions. The observed changes correspond to the decrease in R_{ULV} by about 40 Å over a range of calcium ion concentrations up to 5 mM (Fig. 3a). At the same time, the analysis of appropriate SANS curves (Fig. 1d) reveals the change of almost 2 Å in the case of d_L (Fig. 3b).

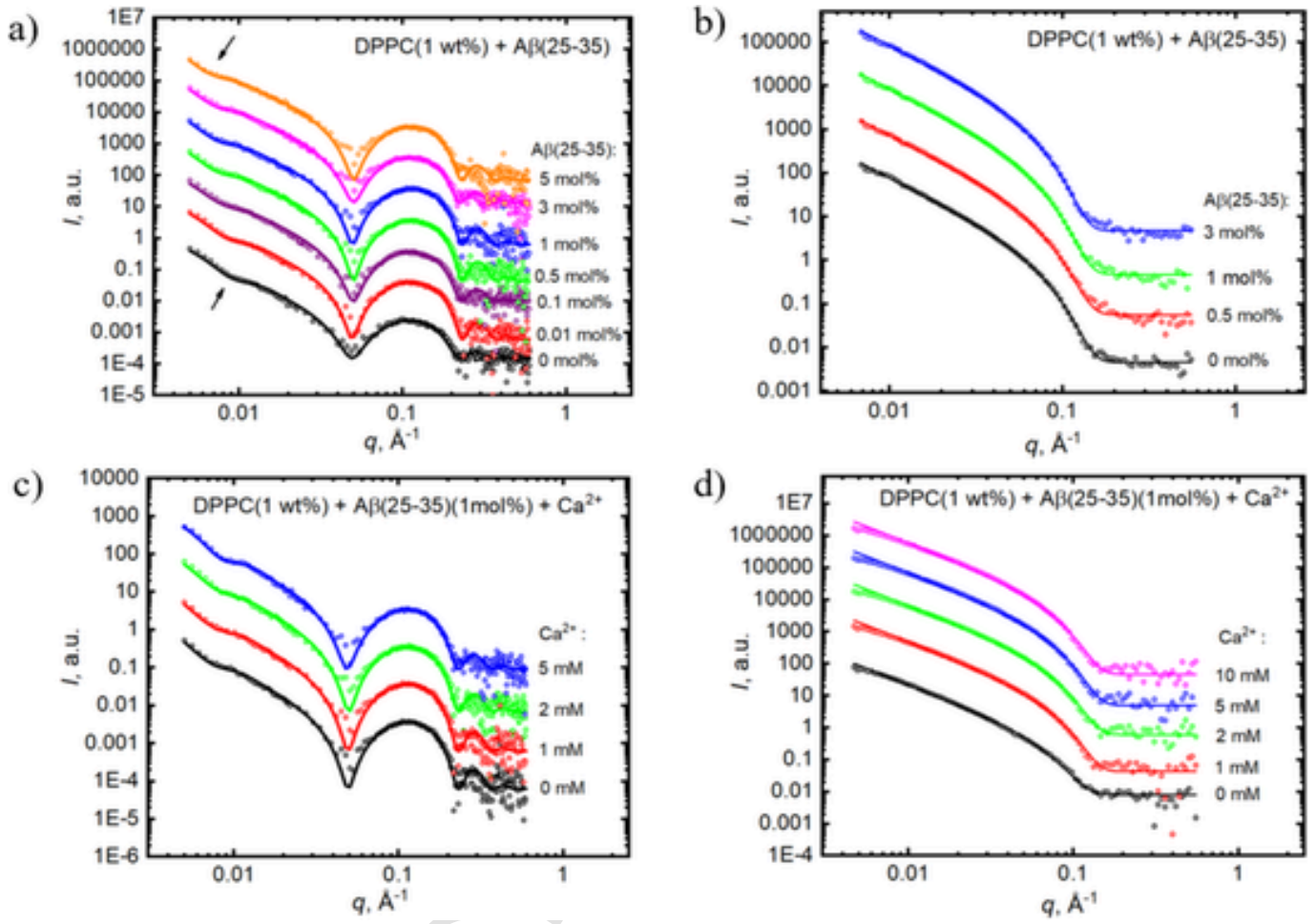

Fig. 1. a) SAXS and b) SANS intensities I as a function of scattering vector q obtained for DPPC(1 wt%) + Aβ (25–35) samples prepared in the form of ULVs and containing different concentrations of Aβ (25–35): 0 mol%, 0.01 mol%, 0.1 mol%, 0.5 mol%, 1 mol%, 3 mol%, 5 mol%. c) SAXS and d) SANS intensities I as a function of scattering vector q obtained for DPPC(1 wt%) + Aβ (25–35)(1 mol%) systems prepared in the form of ULVs and containing different concentrations of calcium ions: 0 mM, 1 mM, 2 mM, 5 mM, while Aβ (25–35) concentration is equal to 1 mol%. All curves were obtained at $T = 20$ °C in the gel phase of DPPC. Full lines represent the best fit results. The curves are shifted vertically for better visualization.

The addition of calcium ions apparently inhibits the impact on membrane structural parameters caused by Aβ (25–35). Several possible mechanisms of inhibition may include changes in peptide conformations, peptide localization or emergence of its clusterization. Unfortunately, our experimental results do not elaborate on the way the calcium ions evoke this effect. We have thus turned to the molecular dynamics simulations, scrutinizing in particular the changes in peptide localization in the lipid membrane due to calcium ion addition. Initially constructed patch of a DPPC lipid bilayer in the gel phase loaded with incorporated peptide molecules, similar system containing calcium ions located initially near the bilayer-water interface, and another system with calcium ions distributed randomly in bulk (Fig. S6) were analyzed after 100 ns of simulation. The electron density distribution functions calculated from the results were averaged over simulation time and appropriate atoms (peptides and lipids separately) (Fig. 4). The results of performed simulations reveal the electron density profiles of the DPPC lipid bilayer and Aβ (25–35) molecules, the last of which remained incorporated into the hydrophobic part of the lipid bilayer without significant differences whether ions are added or not, indicating the absence of changes in the peptide localization within the lipid membrane.

3.2. *Effect of Aβ (25–35) peptides and calcium ions on formation of BLSs*

After the measurements performed above, several of the same DPPC (1 wt%) + Aβ (25–35) samples in the presence and absence of calcium ions were subjected to 3 heating-cooling cycles in a thermobox as described in the Sample preparation section in order to study the Aβ (25–35) driven morphological reorganization of lipid membranes upon addition of calcium ions. Being explained by the Aβ (25–35) induced membrane disruption, the lipid objects are known to be transformed from initially extruded ULVs into bicelle-like structures (BLSs) in the lipid gel phase after crossing T_m upon heating and subsequent cooling of the samples containing Aβ (25–35) (see also Fig. S1) [26–28]. Following the heating-cooling procedure, we have scrutinized the final-state samples at 20 °C in the gel phase of DPPC, as it is the samples in the gel phase that may adopt different shapes (the samples form always the ULVs in the fluid phase [26]). The evaluation was performed by means of SAXS and we compared the results to those obtained for initial-state samples.

Fig. 5 depicts SAXS curves and their fits for DPPC(1 wt%) + Aβ (25–35) samples at various concentrations of Aβ (25–35), as well as those with 2 mM of calcium ions added. After the heating-cooling cycles of the samples, all SAXS curves for samples at the peptide concentration interval of 0–0.5 mol% remained the same as those for initially

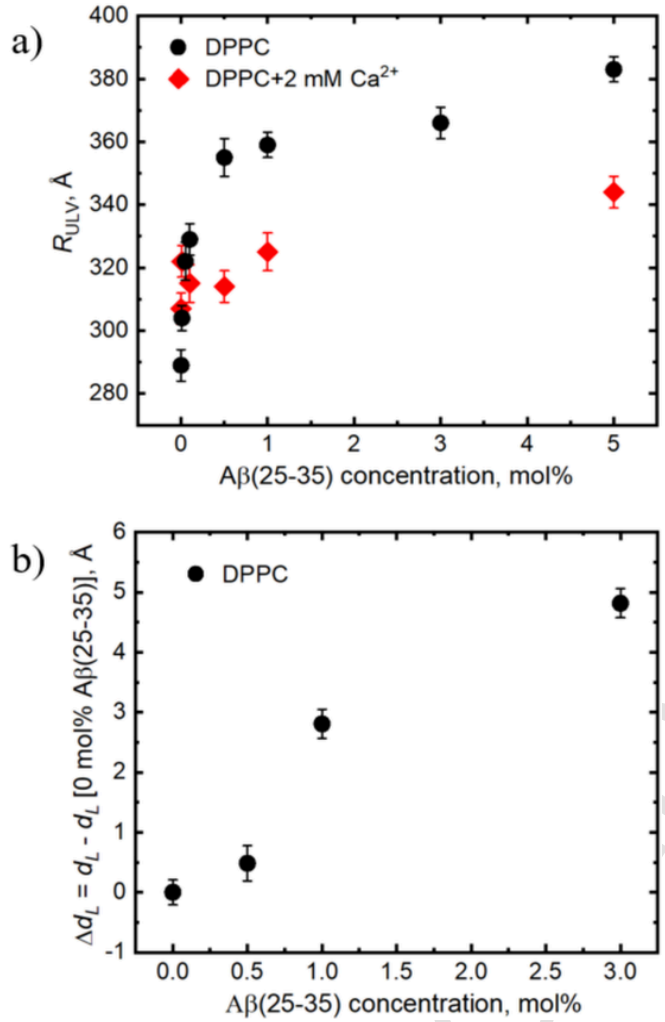

Fig. 2. a) Changes in the radius (R_{ULV}) of ULVs made of DPPC + Aβ (25–35) systems as a function of Aβ (25–35) concentration without calcium ions (black dots) and in the presence of 2 mM calcium ions (red dots). b) Relative changes (Δd_L) to the DPPC lipid bilayer thickness calculated as a difference between d_L of the bilayer with various concentrations of Aβ (25–35) and that of neat DPPC. (For interpretation of the references to colour in this figure legend, the reader is referred to the web version of this article.)

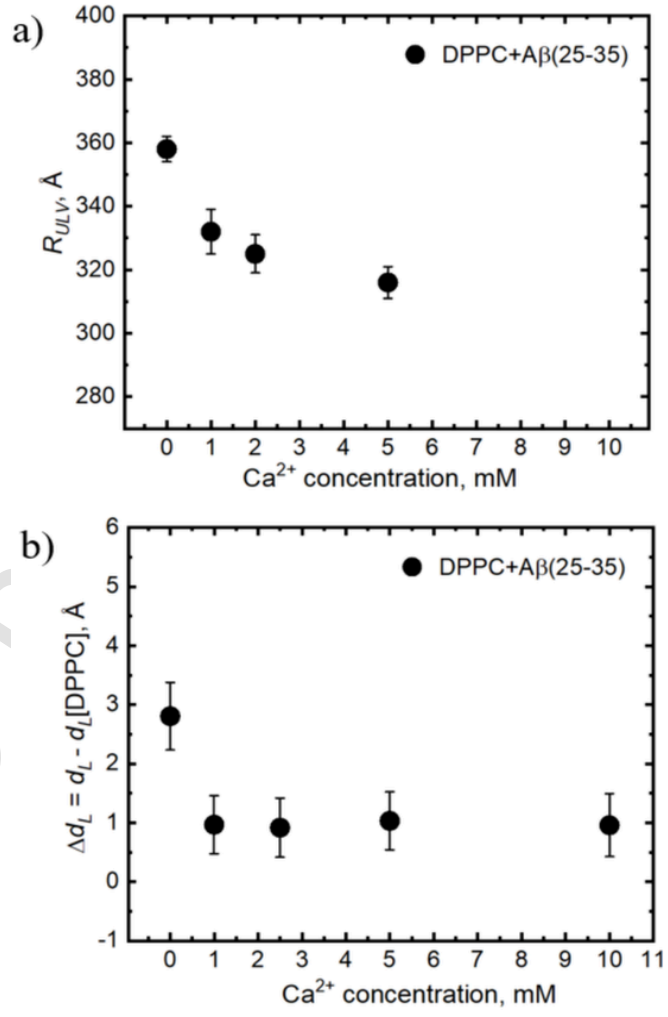

Fig. 3. a) Changes in the radius (R_{ULV}) of ULVs made of DPPC + Aβ (25–35) (1 mol%) upon increasing calcium ion concentration at Aβ (25–35) concentration fixed to 1 mol%. b) Relative changes Δd_L to the DPPC lipid bilayer thickness calculated as a difference between d_L of the DPPC + Aβ (25–35) at various concentrations of calcium ions relative to the system of neat DPPC. All R and d_L values were obtained at $T = 20$ °C in the DPPC gel phase.

extruded ULVs (described in the previous section). However, the curves of the samples (with or without calcium ions) noticeably changed at the peptide concentrations of 1–5 mol%. Namely, these curves show a typical downturn at the low q-range (< 0.01 Å^{-1}) that has been documented previously in the case of disk-shaped objects [26,28]. This interval and the curves in general can be fitted well by the model containing form-factor of a thin disk describing the BLS combined with form-factor of a lipid bilayer represented by 3 G functions (see Supplementary material).

The size-related parameters of emerged objects (radii of the ULVs – R_{ULV} and radii of the BLSs – R_{BLS}) obtained from the fitting analysis of SAXS curves are presented in Fig. 6. In the Aβ (25–35) concentration range of 0–0.5 mol%, the values of R_{ULV} coincide with those of initially extruded ULVs not treated with the heating-cooling cycles (compare empty and full points in Fig. 6). However, the radius of objects changes dramatically from ≈ 360 Å to 200 Å in systems with 1–5 mol% Aβ (25–35), corroborating a ULV-BLS transition. It is important to emphasize that changes of radius and thickness values between ULV and BLS morphologies are in a good agreement with those described in our previous works [26–29]. Hence, we confirm the formation of BLSs in the gel phase of DPPC as a final state of the samples after being heated through T_m with subsequent cooling.

Interestingly, calcium ions at 2 mM concentration do not affect the formation of BLSs (compare black and red points in Fig. 6). The values of R_{BLS} are virtually identical to those of the samples without ions at the same Aβ (25–35) concentrations of 1–5 mol%. This observation suggests a direct interaction of Aβ (25–35) molecules with the lipid membrane in the presence or absence of calcium ions, excluding the scenario of calcium-induced Aβ-aggregation [11,12] outside the lipid bilayer in our study.

Based on our results, we conclude Aβ (25–35) molecules being incorporated into the lipid bilayer at low concentrations (≤ 0.5 mol%) without their ability to launch the chain of morphological reorganizations of lipid membranes. However, achieving a critical peptide concentration allowed the Aβ (25–35) molecules to cause a morphological reorganization of the lipid membrane from the initial ULVs to the final morphology of BLSs. This reorganization and thus a temporal membrane disintegration occurring when crossing T_m is a direct evidence of Aβ-lipid interactions playing a major role in the membrane destruction.

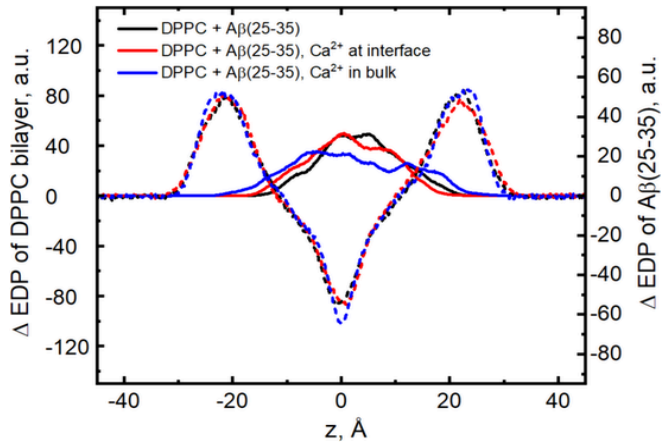

Fig. 4. Relative electron density profiles (ΔEDPs) of a simulated DPPC bilayer (dashed lines; left-hand scale) with incorporated Aβ (25–35) molecules (full lines; right-hand scale) with (red and blue lines) or without (black line) calcium ions added as a function of distance z along the bilayer normal. The ΔEDPs of peptides are enlarged for their better visualization. (For interpretation of the references to colour in this figure legend, the reader is referred to the web version of this article.)

By calling the reorganization temporal disintegration we emphasize that membranes do not get damaged, rather they break and change their shape between two stable membrane morphologies (ULVs and BLSs).

Dysregulations of many cellular processes are known to be affected by the membrane composition, molecular surroundings, and protein concentration. The recent attempts to control membrane fluidity through the addition of cholesterol and melatonin, or introduction of charged lipids did not inhibit the Aβ (25–35) triggered morphological membrane transitions [26–28]. The present results show that the effect is not prevented either upon the addition of calcium ions. Via the progress of eliminating various factors, we can now suggest to examine the impact of other properties of membrane surrounding environment. The solution *pH* in particular, may allow to reveal conditions that are necessary for the mechanism of membrane disruption to take place, and consequently, those that may prevent it.

3.3. Lipid-peptide arrangement of BLSs in the presence of calcium ions

Further, we employed ^{31}P NMR to study the impact of calcium ions on the lipid-peptide arrangement of BLSs. A special arrangement that allows for a stable bicelle-like structure has been documented recently for DPPC(5 wt%) + Aβ (25–35)(1 mol%) systems without calcium ions [29]. Due to the increased lipid concentrations used in NMR, we have extended the range of investigated calcium concentrations in these experiments. Given that lipid/cation ratio varies from 10 to 2 in the range of 1–5 mM calcium ions in the samples with 1 wt% DPPC (SANS and SAXS measurements), we have used calcium concentrations equal to 10 mM and 50 mM for 5 wt% DPPC in order to preserve similar lipid/cation ratios.

DPPC(5 wt%) + Aβ (25–35)(1 mol%) + Ca^{2+} samples treated with 3 heating-cooling cycles prior to measurements, thus being supposedly in the form of BLSs due to the action of 1 mol% Aβ (25–35) [29], were placed in the NMR spectrometer and measured after temperature equilibration. Static ^{31}P NMR spectra recording signals from the lipid head group phosphorus were obtained over the temperature range from 30 °C to 45 °C with gradual heating. Fig. 7 depicts the spectra of DPPC(5 wt%) + Aβ (25–35)(1 mol%) at calcium concentrations of 0, 10, and 50 mM. All spectra distinguish the presence of two phases in the samples – the anisotropic phase in high-field region and a small

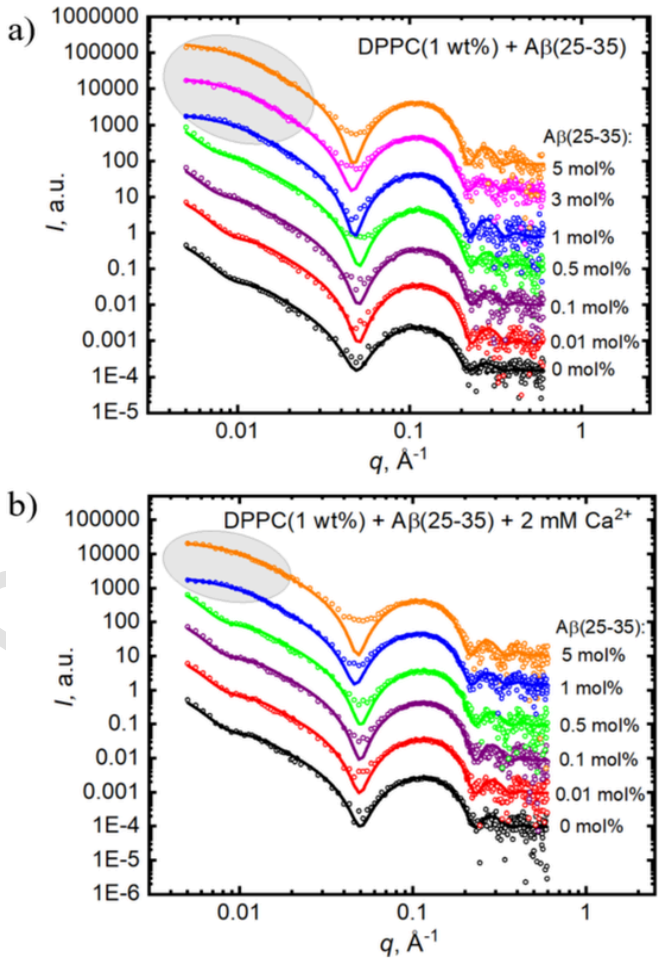

Fig. 5. SAXS intensities I as a function of scattering vector q obtained for a) DPPC(1 wt%) + Aβ (25–35) and b) DPPC(1 wt%) + Aβ (25–35) + 2 mM Ca^{2+} samples being extruded, subsequently subjected to 3 heating-cooling cycles, and measured at T = 20 °C. The different curves correspond to samples with varying concentrations of Aβ (25–35) in accordance to the legend. Solid lines represent the best fits conforming to the models describing ULVs (0–0.5 mol%) and BLSs (1–5 mol%). The circled q range depicts recognizable feature typical for discoidal structures [26]. The curves are shifted vertically for better visualization.

fraction of the isotropic phase at 0 ppm. The anisotropic phase is associated with the magnetic alignment of our BLSs according to our previous findings [29], where the normal to the BLS surface is oriented perpendicular to the magnetic field of the NMR spectrometer. At the same time, the isotropic phase of the samples is related to the fast lipid motions, such as those of small tumbling vesicles or unoriented BLSs.

At low temperatures, the spectra for all studied samples reveal mostly a broad peak in the region of ≈ −15 ppm. As discussed in our previous work [29], the line broadening at these temperatures is most probably caused by a wide angular distribution of BLSs in the magnetic field of NMR spectrometer, although increased spin-spin relaxation of phosphorus and possible undulations of the flat bilayered part of the BLSs can be present in these signals as well. At higher temperatures however, the broad peak is narrowed as a result of the well aligned BLSs. Additionally, it splits into two peaks, which are the most discernible in the DPPC fluid phase at 45 °C (T_m of DPPC ≈ 41 °C [74]). Interestingly, the off zero peaks imply the presence of anisotropic phase even at 45 °C, though the system was supposed to transform from BLSs into small ULVs above the lipid T_m [26–28]. This behavior is however

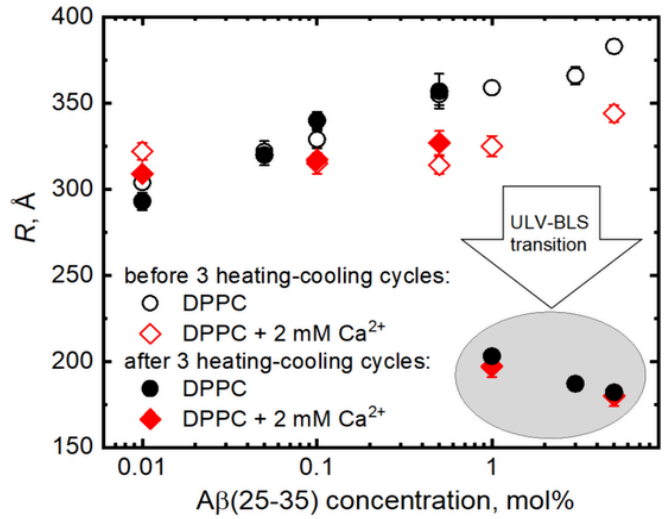

Fig. 6. Radii of ULVs at 0.01–0.5 mol% of Aβ (25–35) and radii of BLSs at 1–5 mol% of Aβ (25–35) in DPPC + Aβ (25–35) systems without calcium ions (black dots) and in the presence of 2 mM calcium ions (red dots) after 3 heating-cooling cycles of initially extruded ULVs (full dots). For the sake of comparison, empty dots display the same samples before heating-cooling cycles. All R values were obtained at T = 20 °C in the DPPC gel phase. The drop of R values at 1–5 mol% of Aβ (25–35) indicates the ULV to BLS transition after heating-cooling cycles performed on ULVs. The circled group of points describes the R_{BLS} values. (For interpretation of the references to colour in this figure legend, the reader is referred to the web version of this article.)

not unexpected in the systems with elevated lipid concentrations, for which the transition may spread over several hours [29].

We take an advantage of delayed transition that results in the well aligned BLSs for resolving their lipid arrangement. We interpret the two peaks in high-field region as the lipid arrangement of our BLSs similar to that of conventional bicelles [75–77] rather than nanodisks [78–80]. Namely, the pronounced peak in the relatively far high-field region is a result of DPPC lipids located at the flat part of the BLSs, while the intermediate peak is associated with the DPPC lipids situated at the perimeter of BLSs and covering the lipid bilayer hydrophobic part. The entire shape of BLSs is supported by Aβ (25–35) molecules localizing predominantly on the rim of BLSs while mixing with lipid molecules [29]. Given that in our present case all ^{31}P NMR spectra for systems containing 0 mM, 10 mM and 50 mM calcium ions demonstrate the same splitting into two peaks, we conclude that the ions affect neither the ability of our BLSs to be well aligned in the magnetic field of NMR spectrometer, nor the lipid arrangement of the BLSs. In addition, peptide localization on the rim of BLSs is likely also unaltered, as the Aβ (25–35) molecules are supposed to be involved in the lipid arrangement at the rim directly [29].

Considering that calcium ions have not affected the overall shape and structure of BLSs, we have also examined the effect of calcium ions on the Aβ (25–35) peptide itself. Namely, we have used circular dichroism to study the secondary structure of Aβ (25–35) molecules in BLSs at various calcium ion concentrations extending our previous research of DMPC(0.5 wt%) + Aβ (25–35) systems [29]. Diluted samples needed for CD spectroscopy have been adapted to the desired relative lipid/ion concentrations in order to compare the results with those of NMR. The CD spectra of DMPC(0.5 wt%) + Aβ (25–35)(3 mol%) samples with added calcium ions are presented in Fig. 8. The spectra were recorded in the state of BLSs at 10 °C, which is below T_m of DMPC ($T_m \approx 24$ °C [74]). The spectrum of DMPC(0.5 wt%) ULVs extruded through the 500 Å filter was subtracted from each of the samples investigated. It is worth noting that the secondary structure of Aβ (25–35) in BLSs is not

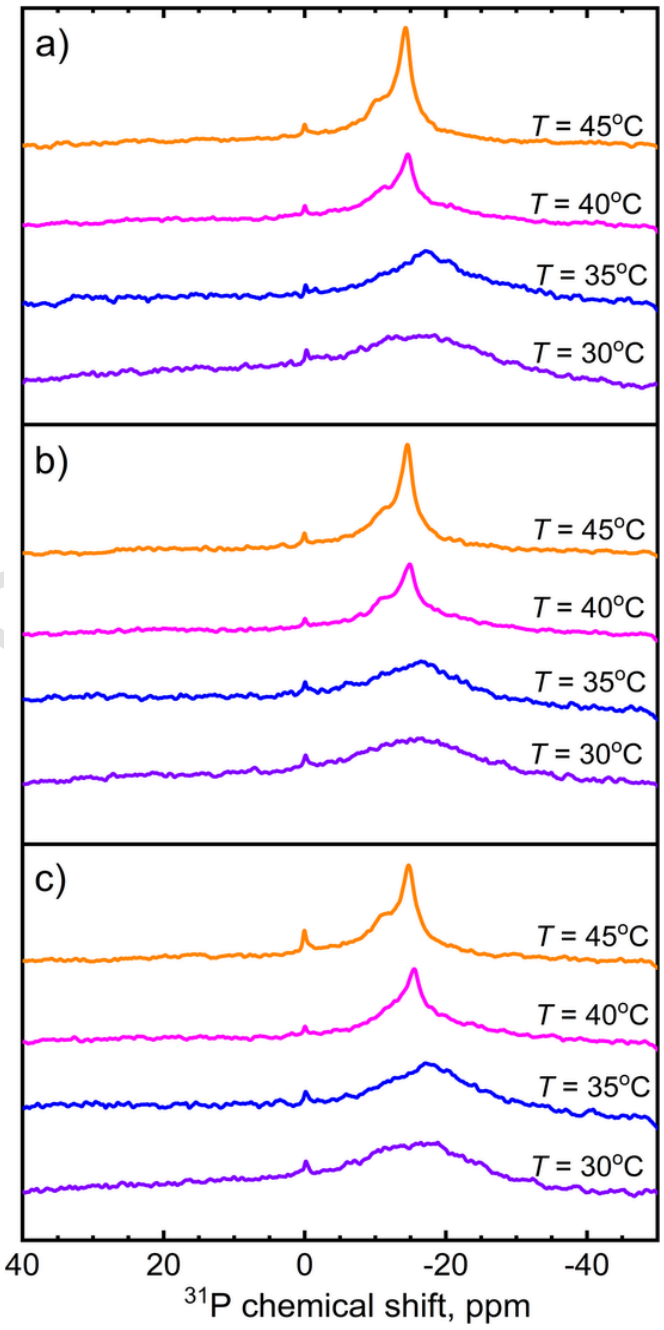

Fig. 7. Static ^{31}P NMR spectra of DPPC(5 wt%) + Aβ (25–35)(1 mol%) samples containing Ca^{2+} ions at concentrations: a) 0 mM, b) 10 mM, c) 50 mM. The spectra were obtained by heating each sample gradually from 30 °C to 45 °C with a step of 5 °C. The anisotropic phase at non-zero resonances is associated with magnetically aligned BLSs.

affected by the choice of saturated lipid (DPPC or DMPC) [26,29], thus we presume that calcium ions would contribute to the secondary structure of Aβ (25–35) incorporated into either DMPC or DPPC membrane equally. The presence of BLSs in the samples used in CD measurements was confirmed by SAXS measurements (not shown).

CD spectra of Aβ (25–35) incorporated into lipid BLSs at 0–0.5 mM Ca^{2+} display a dip at 196 nm and a decline around 210–230 nm. This indicates that secondary structures are predominantly represented by random coils [81,82]. The further increase of calcium ions concentration leads to the spectrum profile changes (1 mM and 5 mM). In partic-

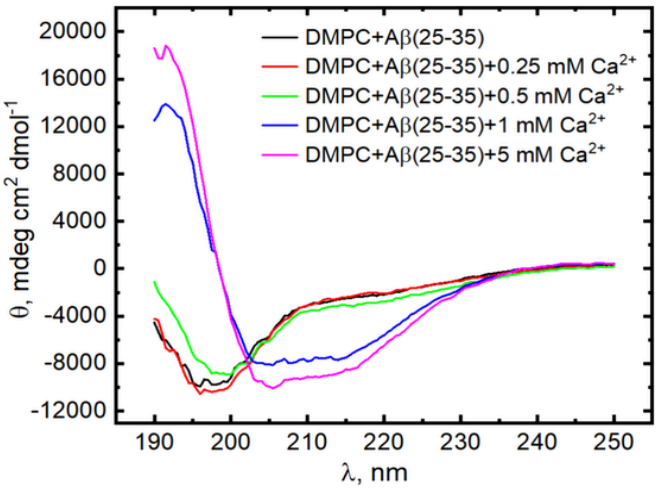

Fig. 8. CD spectra of DMPC(0.5 wt%) + Aβ (25–35)(3 mol%) samples with added calcium ions ranging from 0 to 5 mM concentrations. Samples were measured at 10 °C (gel phase of DMPC) in the state of BLSs.

ular, there is a pronounced maximum around 193 nm and two minima around 205 nm and 217 nm. This behavior of the spectrum may be assumed to indicate the presence of ordered secondary structures in the form of α-helices [81,82].

The fractions of various secondary structures in the samples containing BLSs in the absence and presence of calcium ions was estimated by using SMP180 protein data set [66] from the DichroWeb website [64] reference list via CONTIN [65] analysis program. The calculated content of α-helices in the samples has gradually increased by 15% comparing to the case of DMPC(0.5 wt%) + Aβ (25–35) without ions, whereas the percentage of all remaining secondary structures slightly decreased (Table S1). Hence we conclude, addition of calcium ions contributes to the partial transition of Aβ (25–35) secondary structures to α-helices, which happens most likely due to ion-lipid interactions, as similar transition was not observed in samples without lipid (Fig. S2). It is worth noting that a full-length Aβ-peptide may adopt α-helix in the presence of a zwitterionic lipid bilayer [83,84], including a central hydrophobic region (K16-E22) [85]. Notwithstanding the mechanism of ion actions, their impact does not seem to affect the entire lipid arrangement of BLSs.

We have also examined the secondary structure of Aβ (25–35) at T = 40 °C (Fig. S7) (fluid phase of DMPC, above T_m). Although it is unclear whether the system undertakes the assumed lipid morphology of small ULVs at T = 40 °C [26] upon addition of calcium ions, the CD spectra do not change noticeably compared to those obtained at T = 10 °C. Consequently, the secondary structure of the Aβ (25–35) peptides does not change upon varying the thermodynamic state of the lipid bilayer in agreement with our previous findings [29].

4. Conclusion

Our investigation of model membranes made of fully saturated zwitterionic lipids (DPPC or DMPC) and Aβ (25–35) peptides dispersed in the calcium ion containing solutions reveals the peptide and calcium ion modulated changes in membrane structural parameters. The increasing Aβ (25–35) concentration leads to the increasing membrane thickness and enlarging vesicle sizes, both related likely to the rigidification of gel phase lipid membranes. The addition of calcium ions to the peptide-loaded membranes, in contrary, is prone to inhibit this effect. However, despite of the obstructing effects of calcium ions on the Aβ (25–35)-regulated membrane elasto-mechanic properties, their addition does not eliminate the membrane morphological reorganization triggered by Aβ (25–35) molecules during the main phase transition of lipids. Namely, we have observed the previously reported emergence of bicelle-like structures in the lipid gel phase, advocating thus a temporal membrane disintegration when crossing T_m, despite of adding the calcium ions. We therefore conclude the key lipid-peptide interactions leading to the morphological changes of lipid membranes unaffected by the presence of the ions. Moreover, the lipid-peptide arrangement of resulted BLSs is also unaffected by the presence of the ions and it is represented by Aβ (25–35) molecules and lipids co-located at the BLS rim in the samples with or without the calcium ions added.

CRediT authorship contribution statement

Sergei Kurakin: Writing – review & editing, Writing – original draft, Visualization, Project administration, Methodology, Investigation, Funding acquisition, Formal analysis, Data curation, Conceptualization. **Oleksandr Ivankov:** Writing – review & editing, Validation, Methodology, Data curation. **Ermuhammad Dushanov:** Writing – review & editing, Investigation, Formal analysis. **Tatiana Murugova:** Writing – review & editing, Validation, Project administration. **Elena Ermakova:** Writing – review & editing, Methodology. **Sergey Efimov:** Writing – review & editing, Resources, Methodology. **Timur Mukhametzyanov:** Writing – review & editing, Resources, Methodology. **Svetlana Smerdova:** Writing – review & editing, Validation, Methodology. **Vladimir Klochkov:** Writing – review & editing, Resources, Methodology. **Alexander Kuklin:** Writing – review & editing, Resources, Methodology. **Norbert Kučerka:** Writing – review & editing, Writing – original draft, Supervision, Project administration, Funding acquisition, Conceptualization.

Declaration of competing interest

The authors declare that they have no known competing financial interests or personal relationships that could have appeared to influence the work reported in this paper.

Acknowledgements

This work has been performed with the support of JINR topical plan [themes 04-4-1147-2024 and 04-4-1149-2-2024/2028]. We acknowledge the utilization of facilities of the Center for shared facilities (KFU), instrument base of Physical Chemistry Department of Butlerov Chemistry Institute (KFU), and the computational heterogeneous cluster HybriLIT (JINR). The NMR study was financially supported by the subsidy allocated to Kazan Federal University for the state assignment in the sphere of scientific activities (project FZSM-2023-0012). Additional support was provided for S.K. by grant [AYSS-23-402-06] and for N.K. by grant [VEGA 1/0305/24].

Appendix A. Supplementary data

Supplementary data to this article can be found online at https://doi.org/10.1016/j.bpc.2024.107292.

References

[1] Y. Ling, K. Morgan, N. Kalsheker, Amyloid precursor protein (APP) and the biology of proteolytic processing: relevance to Alzheimer's disease, Int. J. Biochem. Cell Biol. 35 (2003) 1505–1535.
[2] G.-F. Chen, T.-H. Xu, Y. Yan, Y.-R. Zhou, Y. Jiang, K. Melcher, H.E. Xu, Amyloid beta: structure, biology and structure-based therapeutic development, Acta Pharmacol. Sin. 38 (2017) 1205–1235.
[3] T. Kubo, S. Nishimura, Y. Kumagae, I. Kaneko, In vivo conversion of racemized β-amyloid ([D-Ser26]Aβ1–40) to truncated and toxic fragments ([D-Ser26]Aβ25–35/40) and fragment presence in the brains of Alzheimer's patients, J. Neurosci. Res. 70 (2002) 474–483.
[4] M. Naldi, J. Fiori, M. Pistolozzi, A.F. Drake, C. Bertucci, R. Wu, K. Mlynarczyk, S.

Filipek, A. De Simone, V. Andrisano, Amyloid β-peptide 25–35 self-assembly and its inhibition: a model undecapeptide system to gain atomistic and secondary structure details of the Alzheimer's disease process and treatment, ACS Chem. Neurosci. 3 (2012) 952–962.
[5] G. Wei, A.I. Jewett, J.-E. Shea, Structural diversity of dimers of the Alzheimer amyloid-β(25–35) peptide and polymorphism of the resulting fibrils, Phys. Chem. Chem. Phys. 12 (2010) 3622–3629.
[6] L. Millucci, R. Raggiaschi, D. Franceschini, G. Terstappen, A. Santucci, Rapid aggregation and assembly in aqueous solution of Aβ (25–35) peptide, J. Biosci. 34 (2009) 293–303.
[7] A. Cardinale, M. Racaniello, S. Saladini, G. De Chiara, C. Mollinari, M.C. de Stefano, M. Pocchiari, E. Garaci, D. Merlo, Sublethal doses of β-amyloid peptide abrogate DNA-dependent protein kinase activity, J. Biol. Chem. 287 (2012) 2618–2631.
[8] C. Wang, X.-M. Yang, Y.-Y. Zhuo, H. Zhou, H.-B. Lin, Y.-F. Cheng, J.-P. Xu, H.-T. Zhang, The phosphodiesterase-4 inhibitor rolipram reverses Aβ-induced cognitive impairment and neuroinflammatory and apoptotic responses in rats, Int. J. Neuropsychopharmacol. 15 (2012) 749–766.
[9] M.E. Clementi, S. Marini, M. Coletta, F. Orsini, B. Giardina, F. Misiti, Aβ(31–35) and Aβ(25–35) fragments of amyloid beta-protein induce cellular death through apoptotic signals: role of the redox state of methionine-35, FEBS Lett. 579 (2005) 2913–2918.
[10] H.-H.G. Tsai, J.-B. Lee, Y.-C. Shih, L. Wan, F.-K. Shieh, C.-Y. Chen, Location and conformation of amyloid β(25–35) peptide and its sequence-shuffled peptides within membranes: implications for aggregation and toxicity in PC12 cells, ChemMedChem 9 (2014) 1002–1011.
[11] A.M. Isaacs, D.B. Senn, M. Yuan, J.P. Shine, B.A. Yankner, Acceleration of amyloid β-peptide aggregation by physiological concentrations of calcium, J. Biol. Chem. 281 (2006) 27916–27923.
[12] A. Itkin, V. Dupres, Y.F. Dufrêne, B. Bechinger, J.-M. Ruysschaert, V. Raussens, Calcium ions promote formation of amyloid β-peptide (1–40) oligomers causally implicated in neuronal toxicity of Alzheimer's disease, PLoS ONE 6 (2011) e18250.
[13] I. Slutsky, S. Sadeghpour, B. Li, G. Liu, Enhancement of synaptic plasticity through chronically reduced Ca^{2+} flux during uncorrelated activity, Neuron 44 (2004) 835–849.
[14] E. Smorodina, B. Kav, H. Fatafta, B. Strodel, Effects of ion type and concentration on the structure and aggregation of the amyloid peptide $A\beta_{16-22}$, Proteins: Struct. Funct. Bioinf. (2023) 1–14.
[15] L. Li, H.-J. Tsai, L. Li, X.-M. Wang, Icariin inhibits the increased inward calcium currents induced by amyloid-beta(25-35) peptide in CA1 pyramidal neurons of neonatal rat hippocampal slice, Am. J. Chin. Med. 38 (2010) 113–125.
[16] L. Fedrizzi, E. Carafoli, Ca^{2+} dysfunction in neurodegenerative disorders: Alzheimer's disease, BioFactors 37 (2011) 189–196.
[17] N. Arispe, J. Diaz, S.R. Durell, Y. Shafrir, H.R. Guy, Polyhistidine peptide inhibitor of the Aβ calcium channel potently blocks the Aβ-induced calcium response in cells. Theoretical modeling suggests a cooperative binding process, Biochemistry 49 (2010) 7847–7853.
[18] O. Simakova, N.J. Arispe, Early and late cytotoxic effects of external application of the Alzheimer's Aβ result from the initial formation and function of Aβ ion channels, Biochemistry 45 (2006) 5907–5915.
[19] M.F.M. Sciacca, I. Monaco, C. La Rosa, D. Milardi, The active role of Ca^{2+} ions in Aβ-mediated membrane damage, Chem. Commun. 54 (2018) 3629–3631.
[20] J.B. Strosznajder, A. Zambrzycka, M.D. Kaęprzak, R.P. Strosznajder, Amyloid β peptide 25–35 modulates hydrolysis of phosphoinositides by membrane phospholipase(s) C of adult brain cortex, J. Mol. Neurosci. 12 (1999) 101–109.
[21] J.R. Brorson, V.P. Bindokas, T. Iwama, C.J. Marcuccilli, J.C. Chisholm, R.J. Miller, The Ca^{2+} influx induced by β-amyloid peptide 25–35 in cultured hippocampal neurons results from network excitation, J. Neurobiol. 26 (1995) 325–338.
[22] H.S. Mogensen, D.M. Beatty, S.J. Morris, O.S. Jorgensen, Amyloid β-peptide(25-35) changes [Ca^{2+}] in hippocampal neurons, NeuroReport 9 (1998) 1553–1558.
[23] N. Kandel, J.O. Matos, S.A. Tatulian, Structure of amyloid β_{25-35} in lipid environment and cholesterol-dependent membrane pore formation, Sci. Rep. 9 (2019) 2689.
[24] N. Kučerka, M.P. Nieh, J. Katsaras, Fluid phase lipid areas and bilayer thicknesses of commonly used phosphatidylcholines as a function of temperature, Biochim. Biophys. Acta 2011 (1808) 2761–2771.
[25] A. Kuklin, D. Zabelskii, I. Gordeliy, J. Teixeira, A. Brûlet, V. Chupin, V. Cherezov, V. Gordeliy, On the origin of the anomalous behavior of lipid membrane properties in the vicinity of the chain-melting phase transition, Sci. Rep. 10 (2020) 5749.
[26] O. Ivankov, T.N. Murugova, E.V. Ermakova, T. Kondela, D.R. Badreeva, P. Hrubovčák, D. Soloviov, A. Tsarenko, A. Rogachev, A.I. Kuklin, N. Kučerka, Amyloid-beta peptide (25–35) triggers a reorganization of lipid membranes driven by temperature changes, Sci. Rep. 11 (2021) 21990.
[27] O. Ivankov, D.R. Badreeva, E.V. Ermakova, T. Kondela, T.N. Murugova, N. Kučerka, Anionic lipids modulate little the reorganization effect of amyloid-beta peptides on membranes, Gen. Physiol. Biophys. 42 (2023) 59–66.
[28] O. Ivankov, T. Kondela, E.B. Dushanov, E.V. Ermakova, T.N. Murugova, D. Soloviov, A.I. Kuklin, N. Kučerka, Cholesterol and melatonin regulated membrane fluidity does not affect the membrane breakage triggered by amyloid-beta peptide, Biophys. Chem. 298 (2023) 107023.
[29] S. Kurakin, D. Badreeva, E. Dushanov, A. Shutikov, S. Efimov, A. Timerova, T. Mukhametzyanov, T. Murugova, O. Ivankov, K. Mamatkulov, G. Arzumanyan, V. Klochkov, N. Kučerka, Arrangement of lipid vesicles and bicelle-like structures formed in the presence of Aβ(25–35) peptide, Biochim. Biophys. Acta Biomembr. 1866 (2024) 184237.
[30] N. Královič-Kanjaková, A. Asi Shirazi, L. Hubčík, M. Klacsová, A. Keshavarzi, J.C. Martínez, S. Combet, J. Teixeira, D. Uhríková, Polymyxin B-enriched exogenous lung surfactant: thermodynamics and structure, Langmuir 40 (2024) 6847–6861.
[31] T. Harayama, H. Riezman, Understanding the diversity of membrane lipid composition, Nat. Rev. Mol. Cell Biol. 19 (2018) 281–296.
[32] M. Söderberg, C. Edlund, K. Kristensson, G. Dallner, Fatty acid composition of brain phospholipids in aging and in Alzheimer's disease, Lipids 26 (1991) 421–425.
[33] M. Martínez, I. Mougan, Fatty acid composition of human brain phospholipids during normal development, J. Neurochem. 71 (1998) 2528–2533.
[34] J. Kang, H.-G. Lemaire, A. Unterbeck, J.M. Salbaum, C.L. Masters, K.-H. Grzeschik, G. Multhaup, K. Beyreuther, B. Müller-Hill, The precursor of Alzheimer's disease amyloid A4 protein resembles a cell-surface receptor, Nature 325 (1987) 733–736.
[35] J. Tang, R.J. Alsop, M. Backholm, H. Dies, A.-C. Shi, M.C. Rheinstädter, Amyloid-β_{25-35} peptides aggregate into cross-β sheets in unsaturated anionic lipid membranes at high peptide concentrations, Soft Matter 12 (2016) 3165–3176.
[36] M.A. Gruden, T.B. Davidova, M. Mališauskas, R.D.E. Sewell, N.I. Voskresenskaya, K. Wilhelm, E.I. Elistratova, V.V. Sherstnev, L.A. Morozova-Roche, Differential neuroimmune markers to the onset of Alzheimer's disease neurodegeneration and dementia: autoantibodies to Aβ(25–35) oligomers, S100b and neurotransmitters, J. Neuroimmunol. 186 (2007) 181–192.
[37] K. Brännström, A. Öhman, M. Lindhagen-Persson, A. Olofsson, Ca^{2+} enhances Aβ polymerization rate and fibrillar stability in a dynamic manner, Biochem. J. 450 (2013) 189–197.
[38] D. Uhríková, N. Kučerka, J. Teixeira, V. Gordeliy, P. Balgavy, Structural changes in dipalmitoylphosphatidylcholine bilayer promoted by Ca^{2+} ions: a small-angle neutron scattering study, Chem. Phys. Lipids 155 (2008) 80–89.
[39] N. Kučerka, E. Dushanov, K.T. Kholmurodov, J. Katsaras, D. Uhríková, Calcium and zinc differentially affect the structure of lipid membranes, Langmuir 33 (2017) 3134–3141.
[40] N. Kucerka, E. Ermakova, E. Dushanov, K.T. Kholmurodov, S. Kurakin, K. Zelinska, D. Uhríkova, Cation-zwitterionic lipid interactions are affected by the lateral area per lipid, Langmuir (2021).
[41] G. Pabst, A. Hodzic, J. Štrancar, S. Danner, M. Rappolt, P. Laggner, Rigidification of neutral lipid bilayers in the presence of salts, Biophys. J. 93 (2007) 2688–2696.
[42] J. Seelig, A. Seelig, Lipid conformation in model membranes and biological membranes, Q. Rev. Biophys. 13 (1980) 19–61.
[43] J. Seelig, Interaction of phospholipids with Ca^{2+} ions. On the role of the phospholipid head groups, Cell Biol. Int. Rep. 14 (1990) 353–360.
[44] A. Melcrová, S. Pokorna, S. Pullanchery, M. Kohagen, P. Jurkiewicz, M. Hof, P. Jungwirth, P.S. Cremer, L. Cwiklik, The complex nature of calcium cation interactions with phospholipid bilayers, Sci. Rep. 6 (2016) 38035.
[45] A. Filippov, G. Orädd, G. Lindblom, Effect of NaCl and $CaCl_2$ on the lateral diffusion of zwitterionic and anionic lipids in bilayers, Chem. Phys. Lipids 159 (2009) 81–87.
[46] D. Huster, G. Paasche, U. Dietrich, O. Zschornig, T. Gutberlet, K. Gawrisch, K. Arnold, Investigation of phospholipid area compression induced by calcium-mediated dextran sulfate interaction, Biophys. J. 77 (1999) 879–887.
[47] A.G. Lee, How lipids affect the activities of integral membrane proteins, Biochim. Biophys. Acta Biomembr. 1666 (2004) 62–87.
[48] D. Uhríková, J. Teixeira, A. Lengyel, L. Almásy, P. Balgavý, Formation of unilamellar dipalmitoylphosphatidylcholine vesicles promoted by Ca^{2+} ions: a small-angle neutron scattering study, Spectroscopy 21 (2007) 576282.
[49] S.A. Kurakin, E.V. Ermakova, A.I. Ivankov, S.G. Smerdova, N. Kučerka, The effect of divalent ions on the structure of bilayers in the Dimyristoylphosphatidylcholine vesicles, journal of surface investigation: X-ray, synchrotron and neutron, Techniques 15 (2021) 211–220.
[50] S. Kurakin, O. Ivankov, V. Skoi, A. Kuklin, D. Uhríková, N. Kučerka, Cations do not Alter the membrane structure of POPC—A lipid with an intermediate area, Front. Mol. Biosci. 9 (2022) 926591.
[51] S.-C. Jao, K. Ma, J. Talafous, R. Orlando, M.G. Zagorski, Trifluoroacetic acid pretreatment reproducibly disaggregates the amyloid β-peptide, Amyloid 4 (1997) 240–252.
[52] I. Bressler, J. Kohlbrecher, A.F. Thunemann, SASfit: a tool for small-angle scattering data analysis using a library of analytical expressions, J. Appl. Crystallogr. 48 (2015) 1587–1598.
[53] A.I. Kuklin, A.I. Ivankov, D.V. Soloviov, A.V. Rogachev, Y.S. Kovalev, A.G. Soloviev, A.K. Islamov, M. Balasoiu, A.V. Vlasov, S.A. Kutuzov, A.P. Sirotin, A.S. Kirilov, V.V. Skoi, M.I. Rulev, V.I. Gordeliy, High-throughput SANS experiment on two-detector system of YuMO spectrometer, J. Phys. Conf. Ser. 994 (2018) 012016.
[54] V.D. Anan'ev, A.A. Belyakov, M.V. Bulavin, A.E. Verkhoglyadov, S.A. Kulikov, K.A. Mukhin, E.P. Shabalin, Cold neutron moderator on an upgraded IBR-2 reactor: the first set of results, Tech. Phys. 59 (2014) 283–286.
[55] A.G. Soloviev, T.M. Solovjeva, O.I. Ivankov, D.V. Soloviov, A.V. Rogachev, A.I. Kuklin, SAS program for two-detector system: seamless curve from both detectors, J. Phys. Conf. Ser. 848 (2017) 012020.
[56] L.A. Feigin, D.I. Svergun, Structure Analysis by Small-Angle X-Ray and Neutron Scattering, Springer, Boston, MA, 1987.
[57] D.M. Sadler, F. Reiss-Husson, E. Rivas, Thickness measurements of single walled dimyristoyl phosphatidylcholine vesicles by neutron scattering, Chem. Phys. Lipids 52 (1990) 41–48.
[58] D. Van Der Spoel, E. Lindahl, B. Hess, G. Groenhof, A.E. Mark, H.J.C. Berendsen, GROMACS: fast, flexible, and free, J. Comput. Chem. 26 (2005) 1701–1718.
[59] J.B. Klauda, R.M. Venable, J.A. Freites, J.W. O'Connor, D.J. Tobias, C. Mondragon-Ramirez, I. Vorobyov, A.D. MacKerell Jr, R.W. Pastor, Update of the CHARMM all-atom additive force field for lipids: validation on six lipid types, J.

Phys. Chem. B 114 (2010) 7830–7843.
[60] W. Humphrey, A. Dalke, K. Schulten, VMD: Visual molecular dynamics, J. Mol. Graph. 14 (1996) 33–38.
[61] E.F. Pettersen, T.D. Goddard, C.C. Huang, G.S. Couch, D.M. Greenblatt, E.C. Meng, T.E. Ferrin, UCSF chimera—a visualization system for exploratory research and analysis, J. Comput. Chem. 25 (2004) 1605–1612.
[62] N. Kučerka, J. Katsaras, J.F. Nagle, Comparing membrane simulations to scattering experiments: introducing the SIMtoEXP software, J. Membr. Biol. 235 (2010) 43–50.
[63] N. Kučerka, J.F. Nagle, J.N. Sachs, S.E. Feller, J. Pencer, A. Jackson, J. Katsaras, Lipid bilayer structure determined by the simultaneous analysis of neutron and X-ray scattering data, Biophys. J. 95 (2008) 2356–2367.
[64] A.J. Miles, S.G. Ramalli, B.A. Wallace, DichroWeb, a website for calculating protein secondary structure from circular dichroism spectroscopic data, Protein Sci. 31 (2022) 37–46.
[65] S.W. Provencher, J. Gloeckner, Estimation of globular protein secondary structure from circular dichroism, Biochemistry 20 (1981) 33–37.
[66] A. Abdul-Gader, A.J. Miles, B.A. Wallace, A reference dataset for the analyses of membrane protein secondary structures and transmembrane residues using circular dichroism spectroscopy, Bioinformatics 27 (2011) 1630–1636.
[67] G. Pabst, M. Rappolt, H. Amenitsch, P. Laggner, Structural information from multilamellar liposomes at full hydration: full q-range fitting with high quality x-ray data, Phys. Rev. E 62 (2000) 4000–4009.
[68] N. Kučerka, Y. Liu, N. Chu, H.I. Petrache, S. Tristram-Nagle, J.F. Nagle, Structure of fully hydrated fluid phase DMPC and DLPC lipid bilayers using X-ray scattering from oriented multilamellar arrays and from unilamellar vesicles, Biophys. J. 88 (2005) 2626–2637.
[69] V. Nele, M.N. Holme, U. Kauscher, M.R. Thomas, J.J. Doutch, M.M. Stevens, Effect of formulation method, lipid composition, and PEGylation on vesicle Lamellarity: a small-angle neutron scattering study, Langmuir 35 (2019) 6064–6074.
[70] M.N. Holme, M.H. Rashid, M.R. Thomas, H.M.G. Barriga, K.L. Herpoldt, R.K. Heenan, C.A. Dreiss, J.L. Bañuelos, H.-N. Xie, I. Yarovsky, M.M. Stevens, Fate of liposomes in the presence of phospholipase C and D: from atomic to supramolecular lipid arrangement, ACS Cent. Sci. 4 (2018) 1023–1030.
[71] S.A. Korono, J.F. Nagle, Closer look at the calorimetric lower transition in lipid bilayers, Chem. Phys. Lipids 259 (2024) 105366.
[72] S. Choi, B. Kang, E. Yang, K. Kim, M.K. Kwak, P.-S. Chang, H.-S. Jung, Precise control of liposome size using characteristic time depends on solvent type and membrane properties, Sci. Rep. 13 (2023) 4728.
[73] T. Kondela, E. Dushanov, M. Vorobyeva, K. Mamatkulov, E. Drolle, D. Soloviov, P. Hrubovčák, K. Kholmurodov, G. Arzumanyan, Z. Leonenko, N. Kučerka, Investigating the competitive effects of cholesterol and melatonin in model lipid membranes, Biochim. Biophys. Acta Biomembr. 1863 (2021) 183651.
[74] D. Marsh, Handbook of Lipid Bilayers, 2nd ed., CRC Press, Taylor & Francis Group, Routledge, 2013.
[75] M.N. Triba, D.E. Warschawski, P.F. Devaux, Reinvestigation by phosphorus NMR of lipid distribution in bicelles, Biophys. J. 88 (2005) 1887–1901.
[76] E.J. Dufourc, Bicelles and nanodiscs for biophysical chemistry, Biochim. Biophys. Acta Biomembr. 1863 (2021) 183478.
[77] K. Yamamoto, P. Pearcy, A. Ramamoorthy, Bicelles exhibiting magnetic alignment for a broader range of temperatures: a solid-state NMR study, Langmuir 30 (2014) 1622–1629.
[78] T. Ravula, J. Kim, D.-K. Lee, A. Ramamoorthy, Magnetic alignment of polymer Nanodiscs probed by solid-state NMR spectroscopy, Langmuir 36 (2020) 1258–1265.
[79] B. Krishnarjuna, G. Sharma, S.-C. Im, R. Auchus, G.M. Anantharamaiah, A. Ramamoorthy, Characterization of nanodisc-forming peptides for membrane protein studies, J. Colloid Interface Sci. 653 (2024) 1402–1414.
[80] C. Anada, K. Ikeda, A. Egawa, T. Fujiwara, H. Nakao, M. Nakano, Temperature- and composition-dependent conformational transitions of amphipathic peptide–phospholipid nanodiscs, J. Colloid Interface Sci. 588 (2021) 522–530.
[81] Y.-H. Chen, J.T. Yang, H.M. Martinez, Determination of the secondary structures of proteins by circular dichroism and optical rotatory dispersion, Biochemistry 11 (1972) 4120–4131.
[82] S.M. Kelly, T.J. Jess, N.C. Price, How to study proteins by circular dichroism, Biochim. Biophys. Acta Proteins Proteom. 1751 (2005) 119–139.
[83] M. Yoda, T. Miura, H. Takeuchi, Non-electrostatic binding and self-association of amyloid β-peptide on the surface of tightly packed phosphatidylcholine membranes, Biochem. Biophys. Res. Commun. 376 (2008) 56–59.
[84] K. Wang, W. Cai, Binding mechanism of full-length Aβ40 peptide to a mixed lipid bilayer, Front. Chem. 12 (2024).
[85] K.J. Korshavn, A. Bhunia, M.H. Lim, A. Ramamoorthy, Amyloid-β adopts a conserved, partially folded structure upon binding to zwitterionic lipid bilayers prior to amyloid formation, Chem. Commun. 52 (2016) 882–885.